Enriched and Discontinuous Galerkin Discretizations for a Cardiac Mechanics Benchmark Problem

Laura Stengel¹, Jonathan Krauß², Axel Loewe², Christian Wieners¹

¹ Institute of Applied and Numerical Mathematics, Karlsruhe Institute of Technology (KIT), Karlsruhe, Germany

² Institute of Biomedical Engineering, Karlsruhe Institute of Technology (KIT), Karlsruhe, Germany

Abstract

Computer models of the human heart enhance understanding of cardiac function but require a compromise between computational cost and numerical accuracy for clinical use. Due to the high mathematical complexity of the underlying model, the commonly used finite element discretization may not achieve the optimal balance between efficiency, reliability, and accuracy. To investigate the impact of different spatial discretization schemes on cardiac mechanics, we realized a benchmark configuration, which considers the hyper-elastic problem of inflating and actively contracting an idealized left ventricle with transversely isotropic and nearly incompressible properties. Comparing linear and quadratic conforming Galerkin, discontinuous Galerkin and enriched Galerkin elements, we found that enriched and discontinuous Galerkin methods reduced locking phenomena but with higher numbers of degrees of freedom and computational costs, particularly for the discontinuous Galerkin approach. However, enriched Galerkin demonstrated comparable robustness to discontinuous Galerkin with substantially fewer degrees of freedom, presenting a favorable compromise between computational efficiency and numerical robustness.

1. Introduction

The cardiac muscle can be modeled by nearly incompressible anisotropic finite elasticity. Let $\Omega \subset \mathbb{R}^3$ be a bounded Lipschitz domain describing the reference geometry of an idealized cardiac ventricle equipped with boundary conditions on the endocardial wall Γ_C and homogeneous Dirichlet boundary conditions on the basal plane Γ_D . Using the elasticity equations for the deformation of a solid in steady-state equilibrium, find the displacement

 ${m u}\colon \Omega o \mathbb{R}^3$ fulfilling

$$\begin{aligned} -\operatorname{div}\left(\boldsymbol{F}\boldsymbol{S}\right) &= \boldsymbol{0}, & \text{in } \Omega, \\ \boldsymbol{u} &= \boldsymbol{0}, & \text{on } \Gamma_{\mathrm{D}}, & \\ \boldsymbol{F}\boldsymbol{S}\boldsymbol{n} &= -p_{\mathrm{C}}\operatorname{Cof}(\boldsymbol{F})\boldsymbol{n}, & \text{on } \Gamma_{\mathrm{C}}, & \end{aligned} \tag{1}$$

with the deformation gradient $F = I_3 + Du$, cf. [1]. We use the second Piola-Kirchhoff stress $S = S_p + T_a f f^{\top}$ decomposed into a passive part S_p and an active part represented by the active stress T_a initiating the active contraction of the tissue. Additionally, we consider the fiber direction f in the reference configuration with |f| = 1. An endocardial pressure load p_C is applied on Γ_C to simulate inflation of Ω . To model anisotropic material properties of biological tissue, we use the nonlinear hyper-elastic transversely isotropic constitutive law by Guccione et al. [2]

$$\widehat{W}_{\text{Gucc}}(\boldsymbol{E}, \boldsymbol{f}) = \frac{1}{2} C_{\text{Gucc}} (\exp(Q(\boldsymbol{E}, \boldsymbol{f})) - 1)$$

with $Q(\boldsymbol{E},\boldsymbol{f})=4c_1(\boldsymbol{f}\cdot\boldsymbol{E}\boldsymbol{f})^2+4c_2|\boldsymbol{E}\boldsymbol{f}|^2+4c_3(\boldsymbol{E}\colon\boldsymbol{E}),$ cf. [3]. The strain energy function depends on the Green-Lagrange strain tensor $\boldsymbol{E}=\frac{1}{2}(\boldsymbol{F}^{\top}\boldsymbol{F}-\boldsymbol{I}_3),$ the fiber direction and the material parameters $C_{\text{Gucc}},b_f,b_{f,s},b_s$ and using $c_1=\frac{1}{4}(b_f-2b_{f,s}+b_s),\ c_2=\frac{1}{2}(b_{f,s}-b_s)$ and $c_3=\frac{1}{4}b_s.$ Near incompressibility $J=\det\boldsymbol{F}\approx 1$ of the material is approximated by a quasi-incompressible approach with the penalty function $W_{\text{vol}}(J)=\frac{1}{2}(J-1)^2$ characterized by Ciarlet [4, Sect. 4.10], which is complemented by the volumetric penalty $\kappa_{\text{vol}}>0$ and added to the strain energy function, i.e.

$$\widehat{W}(\boldsymbol{E},\boldsymbol{f}) = \widehat{W}_{\text{Gucc}}(\boldsymbol{E},\boldsymbol{f}) + \kappa_{\text{vol}} W_{\text{vol}}(J) \,.$$

2. Methods

Let \mathcal{K}_h be an admissible and uniform triangulation of Ω in tetrahedral elements K with $\overline{\Omega}_h = \bigcup_{K \in \mathcal{K}_h} \overline{K}$ and maximal element diameter $h = \max_{K \in \mathcal{K}_h} \operatorname{diam}(K)$. For a tetrahedron $K \in \mathcal{K}_h$, let $\mathcal{V}_h = \bigcup_{K \in \mathcal{K}_h} \mathbf{V}_K \subset \overline{\Omega}$ be the vertices of the mesh. Let $\mathcal{F}_h = \bigcup_{K \in \mathcal{K}_h} \mathcal{F}_K$ be the faces

in \mathcal{K}_h , with the faces $\mathcal{F}_K = \bigcup_{j=0}^3 F_{K,j}$ on each element $K \in \mathcal{K}_h$. For a face $F \in \mathcal{F}_K$, it is either $F \subset \partial \Omega$ or $\operatorname{int}(F) \subset \Omega$ for all $K \in \mathcal{K}_h$. Therefore, a face $F \subset \overline{\Omega}$ is called a boundary face if there exists an element $K \in \mathcal{K}_h$ such that $F = \partial K \cap \partial \Omega$ is a face of K. For $F \in \mathcal{F}_K \cap \Omega$, the neighboring element $K' \in \mathcal{K}_h$ with $F \in \mathcal{F}_{K'}$ is unambiguously defined. Let $K, K' \in \mathcal{K}_h$ be two distinct elements such that $F = \partial K \cap \partial K'$ and $F \subset \mathcal{F}_K \cap \mathcal{F}_{K'}$. The orientation of the face normal is then given by selecting $\mathbf{n}_F \in \{\mathbf{n}_K, \mathbf{n}_{K'} = -\mathbf{n}_K\}$. Furthermore, let $\mathcal{N}_h \subset \overline{\Omega}$ be the set of all nodal points with N_K being the number of nodal points in a single element $K \in \mathcal{K}_h$ within the used finite element space V_h . In the following, we use

- conforming Galerkin finite elements V_h^{cG} [5],
- discontinuous Galerkin finite elements V_h^{dG} [6],
- enriched Galerkin finite elements $V_h^{\rm eG}$ [7].

Depending on the discretization, we define the total energy and compute a critical point approximating the weak formulation of the nonlinear system (1), cf. [4]. The resulting discretized equation can be solved approximately by Newton's method, where for every iteration k, the residual r^k and the linearization are calculated to solve the linearized problem for $\boldsymbol{u}_h^k \in \boldsymbol{V}_h$

$$a(\boldsymbol{u}_h^k; \boldsymbol{u}_h^{k+1}, \boldsymbol{\theta}_h) = -r^k(\boldsymbol{u}_h^k; \boldsymbol{\theta}_h)$$

for all test functions $\theta_h \in V_h$. Within the Newton iteration, the linearization and the linear problem are solved with a parallel preconditioned GMRES method [8].

2.1. Conforming Galerkin elements

Using element-wise smooth functions, which are continuous along the edges between the elements $K \in \mathcal{K}_h$, the conforming finite element ansatz space is defined by $V_h^{\mathrm{cG}} = \left\{ \phi_h \in \mathrm{C}^0(\overline{\Omega}) \colon \phi_h|_K \in \mathbb{P}_p(K), \ K \in \mathcal{K}_h \right\}$ with p > 0, and we use

$$oldsymbol{V}_{0,h}^{\mathrm{cG}} = \left\{ oldsymbol{\phi}_h \in V_h^{\mathrm{cG},3} \colon oldsymbol{\phi}_h = oldsymbol{0} \ \ \mathrm{on} \ \ \Gamma_{\mathrm{D}}
ight\}.$$

Approximating the hyper-elastic problem with pressure boundary, using the Guccione material with included active stress approach, the discrete nonlinear problem for $\boldsymbol{u}_h \in \boldsymbol{V}_{h.0}^{\text{cG}}$ is solved for all $\boldsymbol{\theta}_h \in \boldsymbol{V}_{h.0}^{\text{cG}}$

$$\int_{\Omega} \mathbf{S}(\mathbf{u}_{h}, T_{a}) : \left(\mathbf{F}_{h}^{\top} \mathbf{D} \boldsymbol{\theta}_{h} \right) d\mathbf{x}$$

$$= - \int_{\Gamma_{c}} p_{\mathbf{C}} \left(\operatorname{Cof}(\mathbf{F}_{h}) \mathbf{n} \right) \cdot \boldsymbol{\theta}_{h} d\mathbf{a}$$
(2)

with $\boldsymbol{F}_h = \boldsymbol{I}_3 + \mathrm{D}\boldsymbol{u}_h$, $\boldsymbol{E}_h = \frac{1}{2} (\boldsymbol{F}_h^{\top} \boldsymbol{F}_h - \boldsymbol{I}_3)$, and stress response $\boldsymbol{S}(\boldsymbol{u}_h, T_\mathrm{a}) = \mathrm{D}_{\boldsymbol{E}} \widehat{W}(\boldsymbol{E}_h, \boldsymbol{f}) + T_\mathrm{a} \boldsymbol{f} \boldsymbol{f}^{\top}$ depending on the active stress T_a . To solve (2), we use Newton's algorithm starting at $\boldsymbol{u}_h^0 \in \boldsymbol{V}_{h,0}^\mathrm{cG}$ and compute the

linearization depending on $m{u}_h \in m{V}_{h,0}^{ ext{cG}}$ and $D_{m{E}}^2 \widehat{W}(m{E}_h, m{f})$

$$\begin{split} a(\boldsymbol{u}_h; & \tilde{\boldsymbol{u}}_h, \boldsymbol{\theta}_h) = \\ & \int_{\Omega} \!\! \left(\mathrm{D}_{\boldsymbol{E}}^2 \widehat{W}(\boldsymbol{E}_h, \boldsymbol{f}) \big[\mathrm{sym} \left(\boldsymbol{F}_h^\top \mathrm{D} \boldsymbol{\theta}_h \right), \mathrm{sym} \left(\boldsymbol{F}_h^\top \mathrm{D} \tilde{\boldsymbol{u}}_h \right) \big] \\ & + \boldsymbol{S} \left(\boldsymbol{u}_h, T_\mathrm{a} \right) : \mathrm{sym} \left(\left(\mathrm{D} \tilde{\boldsymbol{u}}_h \right)^\top \mathrm{D} \boldsymbol{\theta}_h \right) \right) \mathrm{d} \boldsymbol{x} \\ & + \int_{\Gamma_{\mathrm{C}}} p_{\mathrm{C}} \big(\left(\boldsymbol{F}_h \times \mathrm{D} \tilde{\boldsymbol{u}}_h \right) \boldsymbol{n} \big) \cdot \boldsymbol{\theta}_h \, \mathrm{d} \boldsymbol{a} \end{split}$$

for all $\tilde{\boldsymbol{u}}_h$, $\boldsymbol{\theta}_h \in \boldsymbol{V}_{h,0}^{\text{cG}}$ in each step k.

2.2. Discontinuous and enriched Galerkin

The discontinuous ansatz space of piecewise continuous functions is defined by $\boldsymbol{V}_h^{\mathrm{dG}} = \prod_{K \in \mathcal{K}_h} \boldsymbol{V}_K \subset \mathbb{P}_p(\Omega_h, \mathbb{R}^3)$ with polynomial degree p>0. Let $K,~K' \in \mathcal{K}_h$ be two tetrahedral elements sharing a face $F \subset \mathcal{F}_K \cap \mathcal{F}_{K'}$. For the functions from the discontinuous ansatz space, the transition from K to its neighboring element K' is discontinuous. Therefore, different function values are obtained on the edges depending on the element used to approach a point on the face. Hence, instead of the function values, the jump terms with $\boldsymbol{\theta}_K = \boldsymbol{\theta}_h|_K$

$$\llbracket \boldsymbol{\theta}_h \rrbracket_F = \begin{cases} \left(\boldsymbol{\theta}_K - \boldsymbol{\theta}_{K'} \right) \otimes \boldsymbol{n}_K, & F = \partial K \cap \partial K', \\ \boldsymbol{\theta}_K \otimes \boldsymbol{n}_K, & F \in \partial K \cap \partial \Omega \end{cases}$$

and mean values

$$\{\{\boldsymbol{\theta}_h\}\}_F = \begin{cases} \frac{1}{2} (\boldsymbol{\theta}_K + \boldsymbol{\theta}_{K'}), & F = \partial K \cap \partial K', \\ \boldsymbol{\theta}_K, & F = \partial K \cap \partial \Omega \end{cases}$$

of the function on an edge have to be considered. This yields to the first variation

$$r(\boldsymbol{u}_{h};\boldsymbol{\theta}_{h}) = \sum_{K \in \mathcal{K}_{h}} \int_{K} \boldsymbol{S}(\boldsymbol{u}_{h}, T_{a}) : (\boldsymbol{F}_{h}^{\top} \mathrm{D}\boldsymbol{\theta}_{h}) \, \mathrm{d}\boldsymbol{x}$$

$$- \sum_{F \in \mathcal{F}_{h} \setminus \{\Gamma_{C}\}} \int_{F} \left(\{ \{\boldsymbol{F}_{h} \boldsymbol{S}(\boldsymbol{u}_{h}, T_{a}) \} \}_{F} [\![\boldsymbol{\theta}_{h}]\!]_{F} \right) + \sigma [\![\boldsymbol{u}_{h}]\!]_{F} \cdot \{ \{\mathbb{C}(\boldsymbol{F}_{h})[\mathrm{D}\boldsymbol{\theta}_{h}] \} \}_{F} \right) \, \mathrm{d}\boldsymbol{a}$$

$$+ \sum_{F \in \mathcal{F}_{h} \setminus \{\Gamma_{C}\}} \frac{\gamma_{F}}{h} \int_{F} [\![\boldsymbol{u}_{h}]\!]_{F} \cdot [\![\boldsymbol{\theta}_{h}]\!]_{F} \, \mathrm{d}\boldsymbol{a}$$

$$+ \int_{\Gamma_{C}} p_{C} \left(\mathrm{Cof}(\boldsymbol{F}_{h}) \boldsymbol{n} \right) \cdot \boldsymbol{\theta}_{h} \, \mathrm{d}\boldsymbol{a}$$

$$(3)$$

and the second variation for all $u_h,\ ilde{u}_h,\ ilde{\theta}_h\in {m V}_h^{{
m dG}}$

$$a(\boldsymbol{u}_{h}; \tilde{\boldsymbol{u}}_{h}, \boldsymbol{\theta}_{h}) =$$

$$\sum_{K \in \mathcal{K}_{h}} \int_{K} \left(D_{\boldsymbol{E}}^{2} \widehat{W}(\boldsymbol{E}_{h}, \boldsymbol{f}) \left[\operatorname{sym} \left(\boldsymbol{F}_{h}^{\top} D \boldsymbol{\theta}_{h} \right), \operatorname{sym} \left(\boldsymbol{F}_{h}^{\top} D \tilde{\boldsymbol{u}}_{h} \right) \right]$$

$$+ \boldsymbol{S}(\boldsymbol{u}_{h}, T_{a}) : \operatorname{sym} \left(\left(D \tilde{\boldsymbol{u}}_{h} \right)^{\top} D \boldsymbol{\theta}_{h} \right) \right) d\boldsymbol{x}$$

$$- \sum_{F \in \mathcal{F}_{h} \setminus \{ \Gamma_{C} \}} \int_{F} \left(\left\{ \left\{ \mathbb{C} \left(\boldsymbol{F}_{h} \right) \left[D \tilde{\boldsymbol{u}}_{h} \right] \right\} \right\}_{F} \left[\boldsymbol{\theta}_{h} \right]_{F}$$

$$+ \sigma \left[\tilde{\boldsymbol{u}}_{h} \right]_{F} \cdot \left\{ \left\{ \mathbb{C} \left(\boldsymbol{F}_{h} \right) \left[D \boldsymbol{\theta}_{h} \right] \right\} \right\}_{F} \right] d\boldsymbol{a}$$

$$+ \sum_{F \in \mathcal{F}_{h} \setminus \{ \Gamma_{C} \}} \frac{\gamma_{F}}{h} \int_{F} \left[\tilde{\boldsymbol{u}}_{h} \right]_{F} \cdot \left[\boldsymbol{\theta}_{h} \right]_{F} d\boldsymbol{a}$$

$$+ \int_{\Gamma_{C}} p_{C} \left(\left(\boldsymbol{F}_{h} \times D \tilde{\boldsymbol{u}}_{h} \right) \boldsymbol{n} \right) \cdot \boldsymbol{\theta}_{h} d\boldsymbol{a}$$

$$(4)$$

using the identity $\mathbb{C}(F) = \mathrm{D}_F^2 \widehat{W}(F)$, $\sigma \in \{-1, 0, 1\}$ and the penalty parameter $\gamma_F > 0$ depending on the polynomial degree p of the ansatz space and the mesh width h of the discretization. The penalty parameter penalizes the discontinuity proportionally to the jump terms. Furthermore, depending on the choice of σ , this leads to different discontinuous Galerkin variants, namely

- Non-Symmetric Interior Penalty (NSIP),
- Incomplete Interior Penalty Galerkin (IIPG),
- Symmetric Interior Penalty (SIP).

The enriched Galerkin discretization is based on the discontinuous Galerkin formulation but with the ansatz space of the conforming Galerkin discretization $\boldsymbol{V}_h^{\text{cG}}$, enriched with discontinuous piecewise linear functions. That is, the ansatz space is defined by $\boldsymbol{V}^{\text{eG}} = \boldsymbol{V}_h^{\text{dG}} \oplus \boldsymbol{V}_{h,0}^{\text{dG}}$ with

$$egin{aligned} oldsymbol{V}_{h,0}^{\mathsf{dG}} &= \{ oldsymbol{u} \in \mathrm{L}_2(\Omega_h, \mathbb{R}^3) \colon oldsymbol{u}_K = c_K(oldsymbol{x} - oldsymbol{x}_K), \ c_K \in \mathbb{R}, \, orall K \in \mathcal{K}_h \} \,, \end{aligned}$$

where \boldsymbol{x}_K denotes the center of an element $K \in \mathcal{K}_h$. The first and second variation needed for Newton's algorithm to solve (1) follows the same idea as for the discontinuous Galerkin discretization, cf. (3) and (4), and differs only with respect to the ansatz space, which is now $\boldsymbol{V}_h^{\text{eG}}$.

3. Results

We reproduce the well established mechanics benchmark introduced by Land et al. [1], which simulates the inflation and contraction of an idealized ventricle to verify and compare the three spatial discretization schemes. The problem geometry is given as a truncated ellipsoid complemented with fibers as described in [1], see Fig. 2.

The basal plane is fixated in all directions and an endocardial pressure $p_{\rm C}=15\,{\rm kPa}$ is applied. Active contraction is considered as a constant active stress

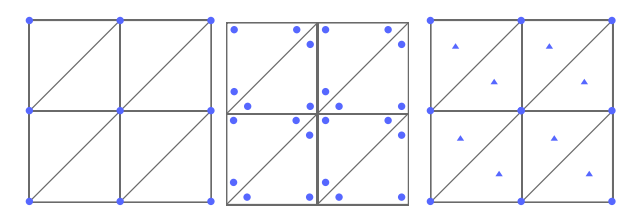


Figure 1: Comparison of DoFs for linear conforming Galerkin (left), discontinuous Galerkin (middle) and enriched Galerkin (right) elements. Here (•) represents two DoFs and (\triangle) represents one DoF.

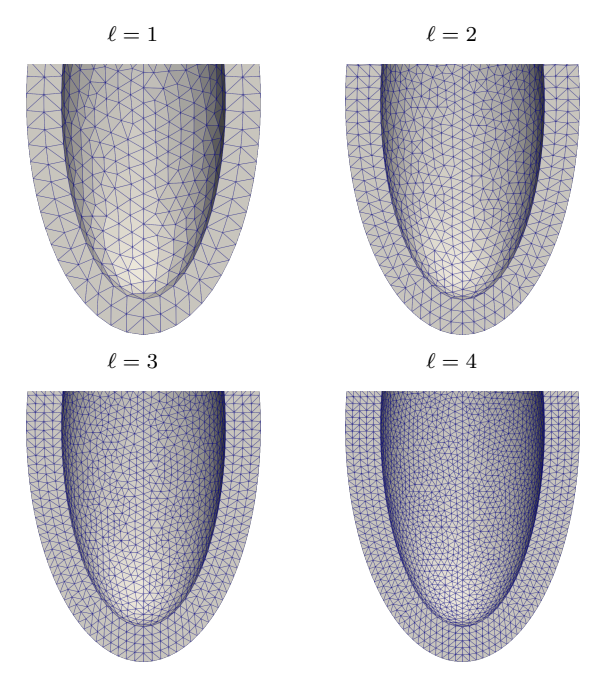


Figure 2: Reference geometry for the active contraction of an idealized ventricle for different mesh refinement levels.

 $T_{\rm a}=60\,{\rm kPa}$ in fiber direction and is simultaneously applied with the pressure. We use the constitutive parameters $C_{\rm Gucc}=2\,{\rm kPa},\ b_{f}=8,\ b_{s}=2,\ b_{f,s}=4$ and $\kappa_{\rm vol}=1\,{\rm MPa}$ to achieve quasi-incompressibility.

We examine the influence of different finite elements by investigating the cavity volume and apico-basal shortening for various mesh refinements ℓ . For the discontinuous and enriched Galerkin discretizations, we used the SIP variant and suitable penalty parameters $\gamma_F^{\rm dG}=2000$ and $\gamma_F^{\rm eG}=200$ determined in numerical experiments using homotopy. In contrast to the conforming Galerkin method, which contains the lowest number of degrees of freedom (DoFs) in these observations, the discontinuous Galerkin finite elements have significantly more DoFs, the enriched Galerkin discretization on the other hand has one additional degree of freedom per element. The discontinuous Galerkin method leads to higher computational costs. For

instance, when running simulations in parallel on 64 processor cores with quadratic conforming and discontinuous Galerkin elements at the finest mesh resolution, the conforming method is roughly 12 times faster. This can be mitigated through homotopy.

Comparing the cavity volume and the apex location in Fig. 3, we observe the occurrence of locking for lowest-order conforming elements and coarse mesh resolutions. This well-known limitation was expected and can be controlled by using higher-order elements or enriched and discontinuous Galerkin elements, see Fig. 3. Besides improving the locking phenomenon even for lowest-order elements using discontinuous and enriched Galerkin, we gain more robustness and stability in contrast to the conforming elements. All introduced finite element discretizations are converging for both the cavity volume and the deformed apex location.

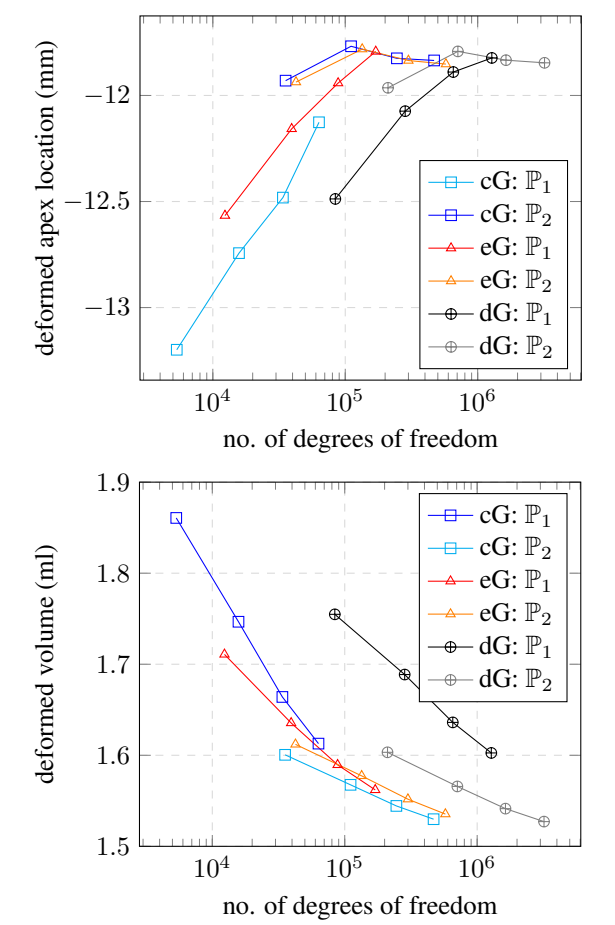


Figure 3: Top: Endocardial apex z-coordinate in the deformed configuration. Bottom: Deformed volume of the simplified, small left ventricle. Both for linear (\mathbb{P}_1) and quadratic (\mathbb{P}_2) elements and different mesh refinements for conforming Galerkin (cG), enriched Galerkin (eG) and discontinuous Galerkin (dG) discretizations.

4. Discussion

All spatial discretizations were converging and within acceptable ranges. Locking for lowest-order conforming finite elements could be improved by using discontinuous or enriched Galerkin elements of the same order, but with a higher number of degrees of freedom. Discontinuous and enriched methods offer crucial implementation choices for optimal performance, including optimal σ or penalty parameter selection. The higher computational time, especially using the discontinuous finite elements, can be reduced by using homotopy. In particular, the nonconforming finite elements showed more stability and robustness. In future, we want to expand our experiments by using a more realistic heart geometry and include coupling to the electrophysiology [9] to manifest our results.

Acknowledgements

This research was funded by the Deutsche Forschungsgemeinschaft (DFG) – Project-ID 258734477 – SFB 1173 and LO 2093/6-1 (SPP 2311) and was supported by bwHPC.

References

- [1] Land S, et al. Verification of cardiac mechanics software: benchmark problems and solutions for testing active and passive material behaviour. Proc R Soc Lond A 2015; 471(2184):2015.0641.
- [2] Guccione JM, et al. Finite element stress analysis of left ventricular mechanics in the beating dog heart. Journal of Biomechanics 1995;28(10):1167–1177.
- [3] Garcia-Blanco E, et al. A new computational framework for electro-activation in cardiac mechanics. Computer Methods in Applied Mechanics and Engineering 2019;348:796–845.
- [4] Ciarlet P. Mathematical elasticity; Volume I. Three-Dimensional elasticity. Studies in mathematics and its applications; v. 20, 27, 29. North-Holland, 1988.
- [5] Braess D. Finite elements: Theory, fast solvers, and applications in solid mechanics. Cambridge University Press, 2001.
- [6] Ten Eyck E, et al. Discontinuous Galerkin methods for nonlinear elasticity. International Journal for Numerical Methods in Engineering 2006;67(9):1204–1243.
- [7] Yi SY, et al. Locking-free enriched galerkin method for linear elasticity. SIAM J Num Anal 2022;60(1):52–75.
- [8] Fröhlich J, et al. Numerical evaluation of elasto-mechanical and visco-elastic electro-mechanical models of the human heart. GAMM Mitteilungen 2023;46(3–4):e202370010.
- [9] Gerach T, Loewe A. Differential effects of mechano-electric feedback mechanisms on whole-heart activation, repolarization, and tension. J Physiol 2024;.

Address for correspondence:

Laura Stengel, IANM3, Karlsruhe Institute of Technology (KIT), Englerstr. 2, 76131 Karlsruhe, Germany (laura.stengel@kit.edu)